Relaxation dynamics of a polymer network modeled by a multihierarchical structure

A. Jurjiu,[1,*] A. Volta,[2,3] and T. Beu[1]

[1]*Universitatea Babes-Bolyai, Faculty of Physics, Simulation Laboratory of Nanostructured Systems, Str. Mihail Kogalniceanu, nr. 1, RO-400084 Cluj-Napoca, Romania*

[2]*Dipartimento di Colture Arboree, University of Bologna, viale Fanin 46, I-40127 Bologna, Italy*

[3]*ARPA-SIMC, Viale Silvani 6, I-40122 Bologna, Italy*

(Received 31 January 2011; revised manuscript received 27 May 2011; published 6 July 2011)

We numerically analyze the scaling behavior of experimentally accessible dynamical relaxation forms for polymer networks modeled by a finite multihierarchical structure. In the framework of generalized Gaussian structures, by making use of the eigenvalue spectrum of the connectivity matrix, we determine the averaged monomer displacement under local external forces as well as the mechanical relaxation quantities (storage and loss moduli). Hence we generalize the known analysis for both classes of fractals to the case of multihierarchical structure, for which even though we have a mixed growth algorithm, the above cited observables still give information about the two different underlying topologies. For very large lattices, reached via an algebraic procedure that avoids the numerical diagonalizations of the corresponding connectivity matrices, we depict the scaling of both component fractals in the intermediate time (frequency) domain, which manifests two different slopes.

DOI: 10.1103/PhysRevE.84.011801 PACS number(s): 36.20.−r, 64.60.al, 64.60.aq, 64.70.km

I. INTRODUCTION

In the last few decades a large and still open issue in polymer physics is the relationship between the geometry of macromolecules and their dynamics. While the first works started from linear polymeric systems [1,2] and their segmental dynamics, [3–5] in recent years attention turned to more and more complex topologies such as star polymers [6–10], dendrimers [6,8–16], hyperbranched polymers [11,13,14,17–22], or small-world networks [23–27]. The concept of fractals introduced by Mandelbrot [28] has turned out to be a useful tool in a large variety of scientific domains, such as disordered systems, growth phenomena, chemical reactions controlled by diffusion, and energy transfer. Far from being merely a geometrical property, the self-similarity of the structure influences significantly the dynamics, from which the important concept of scaling emerges clearly. Fractal lattices are hierarchical structures, i.e., grown by replicating and by connecting a native core through a certain procedure specific to each fractal. When one uses a manifold growth algorithm one obtains a multihierarchical structure. In this way the final structures will appear akin to different fractals depending on the scale on which they are observed.

We perform our calculations in the framework of generalized Gaussian structures (GGSs) [8,9,26,29,30], which are the natural extension of the simple Rouse [1] model to complex geometries. A GGS, being a generalization of the Rouse model, has all the limitations of its predecessor: it does not account for excluded volume interactions nor for entanglement effects. However, one may note that excluded volume effects are often screened. This occurs especially in rather dense media, such as dry polymer networks and polymer melts [4]. The entanglement effects, in turn, are not dominant as long as one stays below the entanglement limit. In the case of polymer networks this means high densities of cross-links, which then implies that the network strands between the cross-link points are rather short. In our model the hydrodynamic interactions are also neglected. The hydrodynamic, solvent-mediated interactions are also generally screened in dense systems [4]. The advantage of using the GGS model is that it allows one, in principle, to determine the full dynamical behavior of the structure through the diagonalization of its connectivity matrix. A GGS consists of beads, connected to each other by elastic springs with elasticity constant K. The unique allowed connections are between nearest neighbor beads, and, for simplicity, it is assumed that all beads experience the same friction constant ζ with respect to the solvent. In this model the solvent (or the surrounding medium) is substituted by a continuous immobile medium which is felt by the network beads through viscous friction and thermal noise. The GGS assumption is that the potential energy [29,30] is built only of harmonic terms, involving monomers directly bound to each other and, also, including interactions with external forces. The connectivity matrix, denoted by $\mathbf{A}$ [4,29,31], plays a key role in investigating the dynamics of the underlying structures. Being the discrete version of the Laplacian operator, the connectivity matrix, $\mathbf{A}$, has found a plethora of applications in many fields of science. It is a real symmetric matrix where the nondiagonal elements A_{nm} equal -1 if the nth and mth beads are directly connected and 0 otherwise, while the diagonal elements A_{mm} equal the number of bonds emanating from the mth bead.

In previous works [20–22,32–35] we have analyzed the scaling behavior for two classes of finite fractals, i.e., the dual Sierpinski gaskets and the Vicsek fractals. Because the topological details of the structure under investigation show up only in limited intermediate regions, which are bounded by large crossover domains, very large fractal structures had to be considered. Using iterative methods to determine the eigenvalues of the connectivity matrix, $\mathbf{A}$, we succeeded in investigating the relaxation behavior for very large fractal

*aurel.jurjiu@phys.ubbcluj.ro

structures (up to 3^{19} beads for dual Sierpinski gaskets with $d = 2$, d being the Euclidean dimension, and up to 4^{13} bead for Vicsek fractals with $f = 3$, where f represents the coordination number) and we showed that for both fractals (in the Rouse case) the dynamical quantities, such as the averaged monomer displacement, relaxation moduli, and dielectric relaxation, scale very well in the intermediate (time or frequency) regime, with slopes which strongly depend on the spectral dimension.

Knowing the individual dynamical behavior of each fractal and being motivated by the search of scaling, the challenge is to create and investigate a new structure which is a combination of both fractals. By replicating the Vicsek fractal in the shape of the dual Sierpinski gasket we have built a new multihierarchical structure. We call it a Vicsek fractal replicated in the shape of the dual Sierpinski gasket (VFRSDSG). Due to geometrical restrictions we strictly used for the construction of the new structure only dual Sierpinski gaskets with $d = 2$ and Vicsek fractals with $f = 3$. The advantage of this multihierarchical structure is that the eigenvalues of its connectivity matrix can be obtained using iterative procedures, allowing us to investigate the relaxation quantities at large generations. Also, the weight of a certain fractal within the structure can be varied by simply changing its generation.

The paper is structured as follows: In Sec. II we briefly discuss the GGSs and the way in which their structures give rise to observable relaxation quantities; we focus on the motion of single GGS monomers under locally acting forces and also on the mechanical relaxation forms of the whole GGS. Section III presents the construction of the multihierarchical structure and the iterative procedure for the determination of the eigenvalues of the topological matrix of the multihierarchical structure. The corresponding relaxation patterns are then determined in Sec. IV. We summarize the conclusions in Sec. V.

II. THEORY

Since the theory of generalized Gaussian structures was explained in detail in previous works [29,30], we summarize here the basic equations and the main formulas concerning the relaxation dynamics patterns. In the Langevin framework, the position vector $\mathbf{R}_n$ of the nth bead of the GGS, subject to an external force $\mathbf{F}_n(t)$, obeys

$$\zeta \frac{d\mathbf{R}_n(t)}{dt} + K \sum_{m=1}^{N} A_{nm}\mathbf{R}_m(t) = \mathbf{f}_n(t) + \mathbf{F}_n(t), \tag{1}$$

where $\zeta = 6\pi\eta_0 a$ is the friction constant of the beads (usually formulated in terms of an effective radius a), $K = 3k_BT/l^2$ is their elasticity constant (where k_B is the Boltzmann constant, T is the temperature, and l^2 is the average length of an isolated bond in thermal equilibrium), and $\mathbf{A} = \{A_{nm}\}$ is the connectivity matrix. The stochastic forces (thermal noise) $\mathbf{f}_n(t)$ are assumed to be Gaussian, with $\langle \mathbf{f}_n \rangle = 0$ and $\langle \mathbf{f}_{n\alpha}(t)\mathbf{f}_{m\beta(t')}\rangle = 2k_BT\zeta\delta_{nm}\delta_{\alpha\beta}\delta(t-t')$ (where α and β denote the x, y, and z directions). A complete solution of the linear system of difference-differential equations given by Eq. (1) is achieved through the diagonalization of the matrix $\mathbf{A}$ (see, e.g., [8,36]), a procedure which involves in general determining both the eigenvalues λ_i and the eigenfunctions of $\mathbf{A}$. We focus on the motion (drift and stretching) of the GGS under a constant external force $\mathbf{F} = F\theta(t-0)\mathbf{e}_y$, switched on at $t = 0$ and acting on a single bead in the y direction. As discussed in [8,24,30,37], the displacement of the bead along the y direction, after averaging both over the fluctuating forces $\mathbf{f}_n(t)$ and over all the beads in the GGS, reads

$$\langle Y(t)\rangle = \frac{Ft}{\zeta N} + \frac{F\tau_0}{\zeta N}\sum_{i=2}^{N}\frac{1-\exp\left[-\frac{\lambda_i t}{\tau_0}\right]}{\lambda_i}, \tag{2}$$

where $\tau_0 = \zeta/K$ and $\lambda_1 = 0$. From Eq. (2) we remark that for the calculation of the averaged monomer displacement we need only the eigenvalues of the connectivity matrix $\mathbf{A}$. We also note that in Eq. (2), due to $\lambda_1 = 0$, the motion of the center of mass has separated automatically from the remaining sum. The behavior of the motion for extremely short and for very long times is obvious: one has in the limit of very short times, from Eq. (2), $\langle Y(t)\rangle \sim Ft/\zeta$, whereas for very long times one reaches $\langle Y(t)\rangle \sim (Ft)/(N\zeta)$. For linear Gaussian chains, in the intermediate time domain, it has been shown [1,4,5,37] that the averaged monomer displacement presents a scaling

$$\langle Y(t)\rangle \sim t^{\gamma}, \tag{3}$$

with $\gamma = 1/2$.

We will also focus on readily measurable quantities for such systems; these are, apart from the above-discussed averaged monomer displacement, also the mechanical relaxation forms. The mechanical part is represented by the complex dynamical modulus $G^*(\omega)$ or, equivalently, by its real $G'(\omega)$ (the storage modulus) and imaginary $G''(\omega)$ (the loss modulus) components [38,39]. For $\omega > 0$, these quantities are given by (see also Eqs. 4.159 and 4.160 of Ref. [4])

$$G'(\omega) = C\frac{1}{N}\sum_{i=2}^{N}\frac{(\omega/2\sigma\lambda_i)^2}{1+(\omega/2\sigma\lambda_i)^2} \tag{4}$$

and

$$G''(\omega) = C\frac{1}{N}\sum_{i=2}^{N}\frac{\omega/2\sigma\lambda_i}{1+(\omega/2\sigma\lambda_i)^2}. \tag{5}$$

For very dilute solutions, one has $C = \nu k_BT$, where ν is the number of polymer segments (beads) per unit volume. For simplicity and without any loss of generality, in the following we set the constants present in Eq. (4) and Eq. (5), which are $C\frac{1}{N}$ and σ, equal to one.

III. STRUCTURE AND EIGENVALUE SPECTRUM

As we have seen in the previous section, the GGSs allow the determination of their main relaxation forms merely by knowing the eigenvalue spectrum. At first glance the procedure looks simple and straightforward: one has only to diagonalize the connectivity matrix $\mathbf{A}$ in order to obtain the eigenvalues and then to use them to calculate the relaxation quantities given by Eqs. (2), (4), and (5). Indeed, it is straightforward for small structures for which the precise numerical diagonalizations of their connectivity matrices are easy to perform. But, as we mentioned in Sec. I, the topological details of the structure under investigation show up only in limited intermediate (time or frequency) domains, which are bounded by large crossover

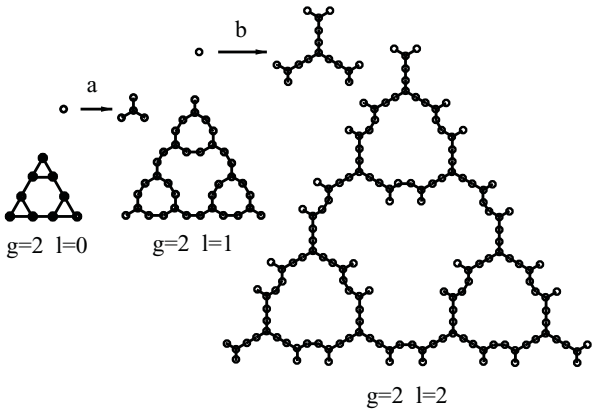

FIG. 1. VFRSDSG structure at generations $g = 2, l = 0$; $g = 2$, $l = 1$; and $g = 2, l = 2$.

domains. In order to extract information about the structure, it is of absolute importance that the size of the structure to be sufficiently large. Evidently, this leads to a quite large connectivity matrix, **A**, whose exact numerical diagonalization is practically impossible to perform.

Fortunately, we have built a multihierarchical structure which has the advantage that the eigenvalue spectrum of its topological matrix can be determined by iterative methods. The multihierarchical structure on which we focus is displayed in Fig. 1 at the generations $g = 2, l = 0$ (only dual Sierpinski gasket); $g = 2, l = 1$; and $g = 2, l = 2$. Throughout this paper, g is the generation of the dual Sierpinski gasket and l is the generation of the Vicsek fractal. The structure is built by replicating the Vicsek fractal in the shape of the dual Sierpinski gasket. Generally, to build the structure at any desired generation g and l, one has first to replace every bead of the dual Sierpinski gasket at generation g with an arrangement of beads in the shape of a Vicsek fractal at generation l and then to connect with springs all these identical arrangements in the dual Sierpinski gasket form. The total number of beads of the dual Sierpinski gasket at generation g is 3^g and the total number of beads of the Vicsek fractal at generation l is 4^l. Because every bead of the dual Sierpinski gasket is replaced with an arrangement of beads in the form of a Vicsek fractal, the total number of the beads of the multihierarchical structure, VFRSDSG, at generation g and l is $N = 3^g \cdot 4^l$.

For a better understanding of the construction we will discuss in the following the cases $g = 2$, $l = 1$ and $g = 2$, $l = 2$ presented in Fig. 1. In order to obtain the VFRSDSG at generation $g = 2$ and $l = 1$ (the middle structure of Fig. 1), first every bead of the dual Sierpinski gasket at generation $g = 2$ (the left-hand-side structure of Fig. 1) is substituted with an arrangement of beads in the form of a Vicsek fractal at generation one (sketched in transformation a) and then all the arrangements are connected with springs in the dual Sierpinski gasket form. In the same manner, but substituting now every bead of the dual Sierpinski gasket at generation $g = 2$ (the left-hand-side structure of Fig. 1) with an arrangement of beads in the shape of a Vicsek fractal at generation two (sketched in transformation b) and reconnecting with springs all the arrangements in the form of a dual Sierpinski gasket, one obtains the multihierarchical structure at generation $g = 2$, $l = 2$, the right-hand-side object of Fig. 1. The continuation is now obvious. It is also very important to observe that when going from generation g and l to generation g and $l + 1$ every bead of the structure at generation g and l is replaced with four new beads arranged in a star-wise fashion in the structure at generation g and $l + 1$. The construction of the dual Sierpinski gaskets and of the Vicsek fractals was presented in previous works [20–22,32–35] and we do not repeat it here. We recall that the fractal and the spectral dimensions for the dual Sierpinski gasket with $d = 2$ are given by

$$\bar{d}_S = \frac{\ln 3}{\ln 2} = 1.58496\ldots \tag{6}$$

and

$$\tilde{d}_S = \frac{2\ln 3}{\ln 5} = 1.36521\ldots \tag{7}$$

and for the Vicsek fractals with $f = 3$ they read

$$\bar{d}_V = \frac{\ln 4}{\ln 3} = 1.26186\ldots \tag{8}$$

and

$$\tilde{d}_V = \frac{2\ln 4}{\ln 12} = 1.15578\ldots. \tag{9}$$

As we mentioned above, the multihierarchical structure, displayed in Fig. 1, has the advantage that the eigenvalues of its connectivity matrix can be determinated using iterative procedures. The iterative methods for the determination of the eigenvalues follow closely the way in which the structure was built. In what follows we present the iterative methods that allow us to obtain the eigenvalue spectrum of the VFRSDSG structure. The determination of the eigenvalues, the solution of

$$(\mathbf{A} - \lambda\mathbf{I})\mathbf{\Phi} = \mathbf{0}, \tag{10}$$

is achieved in two distinct stages. For the structure VFRSDSG at any generation $g \geqslant 1$ and $l \geqslant 1$ the first stage consists in the determination of the eigenvalues spectrum of the dual Sierpinski gasket at generation g. For the dual Sierpinski gasket with $d = 2$ the iterative procedure for the calculation of the eigenvalue spectrum was discussed at length in Ref. [46] and then generalized for any value of d in Ref. [33]. We follow the in-depth analysis of Refs. [33] and [46]. One proceeds as follows: given the eigenvalue spectrum at generation $g - 1$, one obtains the eigenvalues at generation g by, first, assigning to each nonvanishing eigenvalue λ_{g-1} two new eigenvalues $\lambda_g^{\pm}$ through the relation

$$\lambda_g^{\pm} = \frac{5 \pm \sqrt{25 - 4\lambda_{g-1}}}{2}. \tag{11}$$

We note that in this way the degeneracies of λ_{g-1} carry over to λ_g^+ and λ_g^-. Second, to this spectrum we add the eigenvalue 3, with degeneracy $(3^{g-1} + 3)/2$, and the eigenvalue 5, with degeneracy $(3^{g-1} - 1)/2$, as well as the nondegenerate eigenvalue $\lambda_1 = 0$. It is very easy to verify that the total number of eigenvalues at the generation g of the dual Sierpinski gasket is 3^g. We use these eigenvalues as an input for the second stage.

In the second stage we determine the eigenvalue spectrum of the VFRSDSG structure using a method based on a real-space decimation. Here, we follow closely the procedure developed in Refs. [20,21]. At every level of generation,

the multihierarchical structure consists of three types of beads: triple-coordinated beads (with three nearest neighbors), double-coordinated beads, and single-coordinated beads (at the ends of dangling bonds). In the following, we write explicitly Eq. (10) for all types of beads and denote the components of the eigenvector $\mathbf{\Phi}$ by ϕ_j. For a particular triple-coordinated bead one has

$$(3-\lambda)\phi_0 = \sum_{j=1}^{3} \phi_j, \tag{12}$$

where ϕ_0 is the eigenvector component of the triple-coordinated bead and the ϕ_js are the eigenvector components of the nearest neighbors of the triple-coordinated bead; these may themselves be either single- or double-coordinated. The corresponding equation for the double-coordinated bead reads

$$(2-\lambda)\phi_j = \phi_0 + \phi_m, \tag{13}$$

where ϕ_m is the eigenvector component of the double-coordinated neighbor of j. The characteristic eigenvalue equation for the single-coordinated bead is

$$(1-\lambda)\phi_1 = \phi_0, \tag{14}$$

where ϕ_1 denotes the corresponding eigenvector component.

As has been clearly shown in the Appendix of Ref. [21], under real-space renormalization transformations involving the decimations of the triple-coordinated, double-coordinated, and single-coordinated beads, Eqs. (12)–(14) are replaced in the new decimated structure by

$$[3-P(\lambda)]\tilde{\phi}_0 = \sum_{j=1}^{3} \tilde{\phi}_j, \tag{15}$$

$$[2-P(\lambda)]\tilde{\phi}_f = \tilde{\phi}_0 + \tilde{\phi}_m, \tag{16}$$

$$[1-P(\lambda)]\tilde{\phi}_1 = \tilde{\phi}_0, \tag{17}$$

where $\tilde{\phi}_0$, $\tilde{\phi}_1$, $\tilde{\phi}_f$, $\tilde{\phi}_j$, and ϕ_m are the eigenvector components in the decimated structure and $P(\lambda)$ is the polynomial

$$P(\lambda) = \lambda(\lambda-3)(\lambda-4). \tag{18}$$

Important aspects of the decimation method have to be mentioned. In the decimation procedure of the triple-coordinated beads, Eq. (15), only the double-coordinated nearest neighbors beads get eliminated, while the decimation of double-coordinated or dangling beads, Eqs. (17) and (18), implies the elimination of both single- and double-coordinated beads (see the Appendix of Ref. [21]). These transformations, used for decimation of the Vicsek fractal, are also appropriate for the decimation of the multihierarchical structure. Furthermore, the double-coordinated beads formed by connecting with springs two dangling beads belonging to different Vicsek fractals (at the construction of the VFRSDSG structure) obey the same transformation given by Eq. (16). These transformations, Eqs. (15)–(17), allow one to decimate the multihierarchical structure from any generation $g \geqslant 1$ and $l \geqslant 1$ to generation $g \geqslant 1$ and $l = 1$. To have a complete decimation of the structure, i.e., to attain the generation $g \geqslant 1$ and $l = 0$, every three connected Vicsek fractals at generation $l = 1$ have to be reduced to a dual Sierpinski gasket at generation $g = 1$. The details of the transformation are presented in the Appendix.

The eigenvalue equation is

$$[2-P(\lambda)]\phi_1' = \phi_2' + \phi_3', \tag{19}$$

where ϕ_1', ϕ_2', and ϕ_3' are the eigenvectors components of the beads from the dual Sierpinski gasket at the stage $g = 1$ and $P(\lambda)$ is the polynomial given by Eq. (18). As can be seen from the Appendix, the eigenvector components from Eq. (19) are, in fact, the sums of four eigenvector components, one component corresponding to the central bead (triple-coordinated) and three components corresponding to its nearest neighbors. Equations (15)–(17) and (19) allow one to iterate at will the decimation procedure. Starting with $p_1(\lambda) = P(\lambda)$, in the kth iteration $P(\lambda)$ is replaced by $p_k(\lambda) = P[p_{k-1}(\lambda)]$. This means that a part of the eigenvalues of the VFRSDSG structure at generation g and l is connected with the eigenvalues at generation g and $l-1$ through the relation

$$P(\lambda_i^{(g,l)}) = \lambda_i^{(g,l-1)}. \tag{20}$$

Note that in this way each previous eigenvalue $\lambda_i^{g,l-1} \neq 0$ gives rise to three new ones. by setting $P(\lambda) = a$, Eq. (18) reads

$$\lambda^3 - 7\lambda^2 + 12\lambda - a = 0. \tag{21}$$

Equation. (21) can be solved analytically by introducing

$$p = \frac{13}{3}, \tag{22}$$

$$q = \frac{70}{27}, \tag{23}$$

$$\rho = |p/3|^{3/2}. \tag{24}$$

The roots of Eq. (21) are given by the Cardano-solution [47]

$$\lambda_\nu^{g,l} = \frac{7}{3} + 2\rho^{1/3}\cos\left(\frac{\mu + 2\pi\nu}{3}\right), \tag{25}$$

with $\nu \in 1,2,3$, where

$$\mu = \arccos\left(\frac{a-q}{2\rho}\right). \tag{26}$$

More specifically, at a stage g and l of the multihierarchical structure, a part of the eigenvalue spectrum is calculated from the eigenvalues of stage g and $l-1$ based on Eq. (21), where the constant a is evidently identified with all $\lambda_{g,l-1}$s (except for the vanishing eigenvalue $\lambda_1 = 0$). These eigenvalues are complemented by the nondegenerate vanishing eigenvalue $\lambda_1 = 0$, the nondegenerate eigenvalue 4, $\Delta_1^{g,l}$ degenerate eigenvalues equal to 1 each, and $\Delta_3^{g,l}$ degenerate eigenvalues equal to 3 each, where the degeneracies $\Delta_1^{g,l}$ and $\Delta_3^{g,l}$ are given by

$$\Delta_1^{g,l} = 3^g(1+4^{l-1}) - \frac{3}{2}(3^g - 1) \tag{27}$$

and

$$\Delta_3^{g,l} = \frac{3^g - 1}{2}. \tag{28}$$

We mention in passing that at the first generation of the structure (i.e., the generation g and $l = 1$) a part of the eigenvalue spectrum is determined from the eigenvalues of the dual Sierpinski gasket at stage g by making use of Eq. (21), where the constant a is identified, of course, with all λ_gs (apart from the eigenvalue $\lambda_1 = 0$). To this eigenvalue

spectrum is added, as mentioned above, the nondegenarate eigenvalues 0 and 4, as well as the degenerate eigenvalues 1 and 3 with their degeneracies $\Delta_1^{g,l}$ and $\Delta_3^{g,l}$ given by Eqs. (27) and (28).

In the determination of the eigenvalue spectrum, special attention should be given to the type of eigenvalues. If, the eigenvalues of the connectivity matrices of the classic fractals, dual Sierpinski gasket, or Vicsek are found to be all persistent (i.e., the eigenvalues appearing at one generation continue to appear in all subsequent generations), then in the case of our multihierarchical structure the eigenvalue spectrum consists of persistent and nonpersistent eigenvalues. The persistent eigenvalues are 1, 3, 4, and equally persistent are all those that are obtained from them in the subsequent generations, based on Eq. (21), as well as the eigenvalue $\lambda_1 = 0$. The nonpersistent eigenvalues are all λ_gs (apart from the vanishing eigenvalue) and all those that are determined from them in the subsequent generations, based on Eq. (21). The nonpersistent eigenvalues appear only at a generation and each, according to Eq. (21), produces three new nonpersistent eigenvalues in the next generation, but they will not continue to appear in subsequent generations. More clearly, the nonpersistent eigenvalues in the first generation of the multihierarchical structure (the generation g and $l = 1$, as said above) are obtained from the λ_gs of the Sierpinski, but none of the λ_gs can be found among the eigenvalues of the generation g and $l = 1$ or further generations. In the second generation, g and $l = 2$, the nonpersistent eigenvalues are determined from all nonpersistent eigenvalues of the first generation and, again, the nonpersistent eigenvalues of the first generation do not appear among the nonpersistent eigenvalues of the second generation nor in subsequent generations. The continuation is now obvious.

Now, it is a simple matter to verify that in this way one obtains at generation g and l a total of $N = 3^g \cdot 4^l$ eigenvalues, which corresponds exactly to the number of beads in the structure. We denote by $N_1^{g,l}$ the total number of eigenvalues obtained from the persistent degenerate eigenvalue 1 (including the eigenvalue 1), with $N_3^{g,l}$ the total number of eigenvalues obtained from the persistent degenerate eigenvalue 3 (including also the eigenvalue 3), with $N_4^{g,l}$ the total number of eigenvalues obtained from the persistent nondegenerate eigenvalue 4 (including the eigenvalue 4), and with $N_S^{g,l}$ the total number of nonpersistent eigenvalues. The expressions for $N_1^{g,l}$ and $N_3^{g,l}$ are

$$N_1^{g,l} = \sum_{i=1}^{l-1} 3^i \Delta_1^{g,l-i}, \tag{29}$$

$$N_3^{g,l} = \sum_{i=1}^{l-1} 3^i \Delta_3^{g,l-i}, \tag{30}$$

which, with $\Delta_1^{g,l}$ and $\Delta_3^{g,l}$ given by Eqs. (27) and (28), become

$$N_1^{g,l} = \sum_{i=1}^{l-1} 3^i \left[3^g (1 + 4^{l-i-1}) - \frac{3}{2}(3^g - 1) \right]$$
$$= 3^g (4^l - 3^l) + \left(\frac{3^l - 1}{2} \right) \left(\frac{3 - 3^g}{2} \right), \tag{31}$$

$$N_3^{g,l} = \sum_{i=1}^{l-1} 3^i \Delta_3^{g,l-i} = \left(\frac{3^l - 1}{2} \right) \left(\frac{3^g - 1}{2} \right). \tag{32}$$

The expressions for $N_4^{g,l}$ and $N_S^{g,l}$ are

$$N_4^{g,l} = \sum_{i=1}^{l-1} 3^i = \frac{3^l - 1}{2}, \tag{33}$$

$$N_S^{g,l} = 3^l (3^g - 1). \tag{34}$$

Hence, the total number of eigenvalues at generation g and l is $N = 1 + N_1^{g,l} + N_3^{g,l} + N_4^{g,l} + N_S^{g,l}$, where the value 1 represents the vanishing eigenvalue $\lambda_1 = 0$. Making use of the Eqs. (31)–(34) one obtains

$$N = 1 + 3^g (4^l - 3^l) + \left(\frac{3^l - 1}{2} \right) \left(\frac{3 - 3^g}{2} \right) + \left(\frac{3^l - 1}{2} \right)$$
$$\times \left(\frac{3^g - 1}{2} \right) + \left(\frac{3^l - 1}{2} \right) + 3^l (3^g - 1) = 3^g \cdot 4^l. \tag{35}$$

IV. RELAXATION PATTERNS

We are now in a position to use the eigenvalues obtained in Sec. III to calculate the different relaxation quantities introduced in Sec. II. We start by focusing on the averaged monomer displacement, $\langle Y(t) \rangle$, given by Eq. (2) in which we set $\tau_0 = 1$ and $F/\zeta = 1$. Figure 2 displays the results obtained for the VFRSDSG structure with generations ranging from $g = 4$ and $l = 4$ to $g = 8$ and $l = 8$; consequently, the total number of beads in the structure varies from $N = 3^4 \cdot 4^4$ to $N = 3^8 \cdot 4^8$. What appears immediately using doubly logarithmic scales of Fig. 2 is that at very short times $\langle Y(t) \rangle \simeq Ft/\zeta$ for all N, whereas at very long times one reaches the domain $\langle Y(t) \rangle \simeq (Ft)/(N\zeta)$, which, in the absence of an external field (based on the Einstein relation for GGS [10]) is the hallmark of simple diffusion. Typical for the topological details of the structure under investigation is the intermediate time domain. We know, from previous works concerning fractals, that the intermediate time domain of $\langle Y(t) \rangle$ appears as a straight line with a slope depending

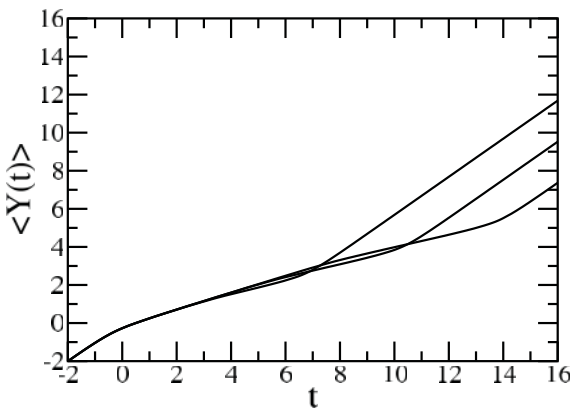

FIG. 2. The averaged monomer displacement under local external forces. Displayed is the normalized $\langle Y(t) \rangle$ for $N = 3^4 \cdot 4^4, 3^6 \cdot 4^6$, and $3^8 \cdot 4^8$, from above, in dimensionless units, evaluated according to Eq. (2).

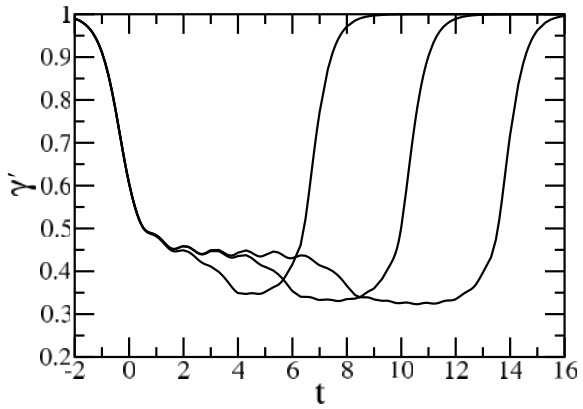

FIG. 3. Slopes γ' of the averaged monomer displacement of Fig. 2, plotted as a function of $\log_{10} t$.

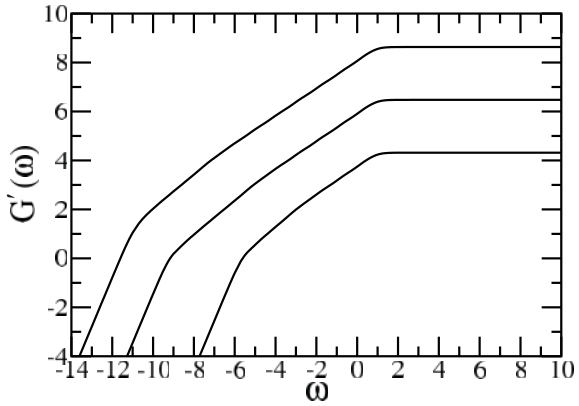

FIG. 4. The normalized storage mudulus $G'(\omega)$ shown in dimensionless units for $N = 3^4 \cdot 4^4, 3^6 \cdot 4^6$, and $3^8 \cdot 4^8$, from below, evaluated according to Eq. (4).

on spectral dimension. Surprisingly, we found that for our multihierarchical structure the intermediate time regime of $\langle Y(t)\rangle$ consists of *two* scaling regions: one corresponding to the component Vicsek fractal of the multihierarchical structure followed at larger intermediate times by another corresponding to the component dual Sierpinski gasket. Furthermore, both scaling behaviors from the intermediate regime obey Eq. (3), with, as we are going to show, γ depending on the spectral dimension of the particular fractal, i.e., $\gamma_V = 1 - \frac{\tilde{d}_V}{2}$ for the Vicsek fractal and $\gamma_S = 1 - \frac{\tilde{d}_S}{2}$ for the dual Sierpinski gasket, respectively.

Now, it is straightforward to determine numerically γ_V and γ_S, which are nothing else than the slopes of the curves in the intermediate time regime. Going from $N = 3^4 \cdot 4^4$ to $N = 3^8 \cdot 4^8$ we have a change in the minimal slopes of the intermediate time regime from $\gamma_V = 0.449$ and $\gamma_S = 0.357$ (for $N = 3^4 \cdot 4^4$) to $\gamma_V = 0.429$ and $\gamma_S = 0.321$ (for $N = 3^8 \cdot 4^8$). The last values should be compared to $\gamma_V = 1 - \frac{\tilde{d}_V}{2} = 0.422$ and $\gamma_S = 1 - \frac{\tilde{d}_S}{2} = 0.317$, where $\tilde{d}_S$ and $\tilde{d}_V$ were calculated from Eqs. (7) and (9). The accuracy attained is certainly enough to assess that the sole parameters of importance are the spectral dimensions of the component fractals of the multihierarchical structure. Moreover, the scaling relations in the intermediate time regime of $\langle Y(t)\rangle$ found in previous works [20,21,32–34] for each fractal (dual Sierpinski gasket and Vicsek fractal) are also maintained for the multihierarchical structure.

In order to render this analysis more quantitative we plot in Fig. 3 the derivative of the curves in Fig. 2. Displayed is the local slope $\gamma' = d \log_{10}(\langle Y(t)\rangle)/d \log_{10}(t)$ as a function of $\log_{10} t$ for the VFRSDSG structure with generations ranging from $g = 4$ and $l = 4$ to $g = 8$ and $l = 8$ awith total number of beads in the structure varying from $N = 3^4 \cdot 4^4$ to $N = 3^8 \cdot 4^8$. In this way one can see clearly in the intermediate time domain the appearance of two plateau regimes. For the largest generation considered, $N = 3^8 \cdot 4^8$, the approximate values of the plateaus are 0.43 and 0.32, in very in good agreement with the values of γ_V and γ_S obtained above. Furthermore, oscillations due to the local structure and multihierarchical construction are also evident.

Most measurements on polymers, however, are not monitored in the time domain but in the frequency domain. Micromanipulation techniques represent an important new experimental development [40–45]. Such techniques allow one to complement macroscopic measurements (such as the determination of the mechanical moduli) by monitoring the microscopic parts of the polymer through their response to forces applied by optical tweezers or by attached magnetic beads. Given the relative ease with which mechanical relaxation measurements can be performed nowadays, we focus on the mechanical moduli $G'(\omega)$ and $G''(\omega)$, given by Eqs. (4) and (5) and presented in Figs. 4 and 5. For the calculation of the relaxation moduli we used again the VFRSDSG structure with generation ranging from $g = 4$ and $l = 4$ to $g = 8$ and $l = 8$; hence, the total number of beads in the structure, N, varies from $3^4 \cdot 4^4$ to $3^8 \cdot 4^8$. In Figs. 4 and 5 we plot Eqs. (4) and (5) in dimensionless units, by setting $\sigma = 1$ and $C/N = 1$. The scales in both figures are doubly logarithmic. Immediately apparent from these figures are the limiting, connectivity-independent behaviors at very small and very large ω; for $\omega \ll 1$ one has $G'(\omega) \sim \omega^2$ and $G''(\omega) \sim \omega$, and for $\omega \gg 1$ one finds $G'(\omega) \sim \omega^0$ and $G''(\omega) \sim \omega^{-1}$. Our main focus is again the regime between the very small and the very high frequencies. Similarly to the case of averaged monomer displacement discussed above, we found, for both $G'(\omega)$ and $G''(\omega)$, that the in-between frequency regime consists of *two* scaling regions: one corresponding to the component Vicsek

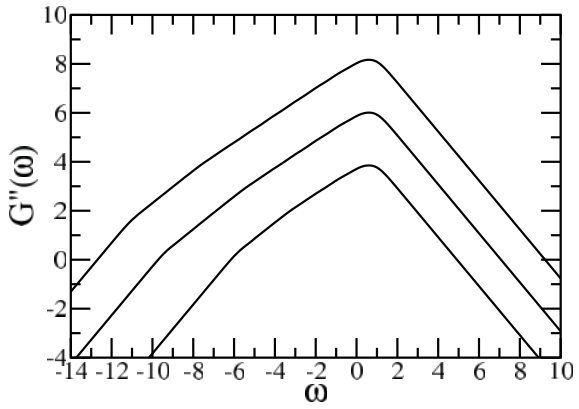

FIG. 5. The normalized loss mudulus $G''(\omega)$ shown in dimensionless units for $N = 3^4 \cdot 4^4, 3^6 \cdot 4^6$, and $3^8 \cdot 4^8$, from below, evaluated according to Eq. (5).

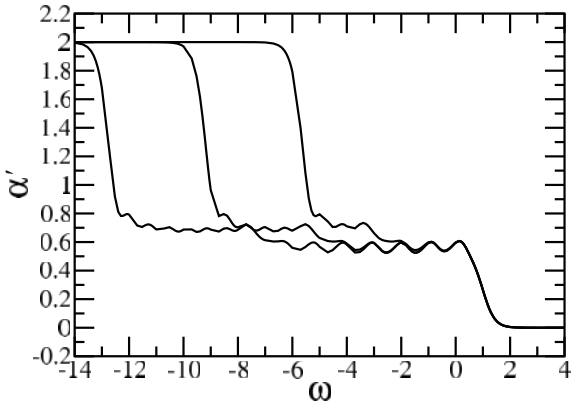

FIG. 6. The effective slopes α' of $G'(\omega)$ of Fig. 4 plotted as a function of $\log_{10}\omega$.

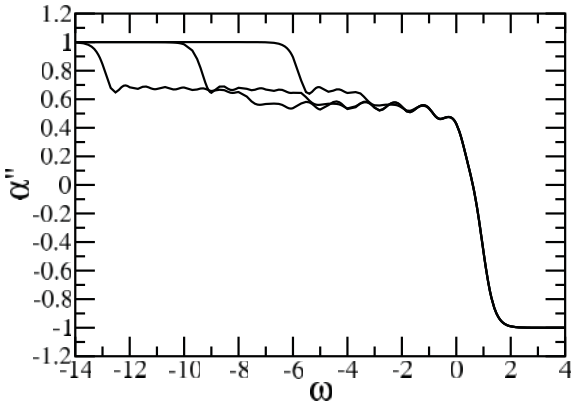

FIG. 7. The effective slopes α'' of $G''(\omega)$ of Fig. 5 plotted as a function of $\log_{10}\omega$.

fractal of the multihierarchical structure followed at larger intermediate frequencies by another corresponding to the component dual Sierpinski gasket. Each of the intermediate scaling regions is dominated by the corresponding spectral dimension. Based on theoretical grounds, we expect the slopes in the intermediate frequency regions to have values equal to half of the corresponding spectral dimension of the region, i.e., $\alpha_V = \frac{\tilde{d}_V}{2}$ and $\alpha_S = \frac{\tilde{d}_S}{2}$. From Fig. 4 we determine for $G'(\omega)$, by going from $N = 3^4 \cdot 4^4$ to $N = 3^8 \cdot 4^8$, the slopes in the intermediate regime as being equal to $\alpha_V = 0.571$ and $\alpha_S = 0.72$ (for $N = 3^4 \cdot 4^4$) and to $\alpha_V = 0.559$ and $\alpha_S = 0.687$ (for $N = 3^8 \cdot 4^8$). The values of the slopes obtained at generation $g = 8$ and $l = 8$ should be compared with the theoretically expected values, $\alpha_V = \frac{\tilde{d}_V}{2} = 0.559$ and $\alpha_S = \frac{\tilde{d}_S}{2} = 0.683$, with $\tilde{d}_S$ and $\tilde{d}_V$ being calculated from Eqs. (7) and (9).

In the same manner, we determine the slopes in the intermediate frequencies regions of $G''(\omega)$. In Fig. 5, going from $N = 3^4 \cdot 4^4$ to $N = 3^8 \cdot 4^8$ we have a change in the minimal slopes of the intermediate frequency regime from $\alpha_V = 0.526$ and $\alpha_S = 0.648$ (for $N = 3^4 \cdot 4^4$) to $\alpha_V = 0.545$ and $\alpha_S = 0.673$ (for $N = 3^8 \cdot 4^8$). Again, the values obtained at generation $g = 8$ and $l = 8$ should be compared with the theoretically expected values, $\alpha_V = \frac{\tilde{d}_V}{2} = 0.559$ and $\alpha_S = \frac{\tilde{d}_S}{2} = 0.683$. We observe that the values of the slopes for $G''(\omega)$ are slightly lower than those for $G'(\omega)$ and that they bound the expected theoretical values from below. On the other hand, the slopes for $G'(\omega)$ tend to the expected theoretical value from above. The main finding is that the scaling relations of mechanical moduli observed in the previous works [20,21,32–34] for each individual fractal still hold for the multihierarchical structure which is a combination of both fractals.

In order to display a more quantitative analysis of the dynamical relaxation we proceed again to plot the quantities $\alpha' = d\log_{10} G'(\omega)/d\log_{10}\omega$ (in Fig. 6) and $\alpha'' = d\log_{10} G''(\omega)/d\log_{10}\omega$ (in Fig. 7) for the VFRSDSG structure with generation ranging from $g = 4$ and $l = 4$ to $g = 8$ and $l = 8$; hence, the total number of beads in the structure, N, varies from $3^4 \cdot 4^4$ to $3^8 \cdot 4^8$. α' and α'' are the derivatives of the curves (i.e., the slopes) of Figs. 4 and 5. Immediately apparent are for very small and for large ω the limiting, theoretically expected values, namely 2 and 0 for α' (in Fig. 6) and 1 and -1 for α'' (in Fig. 7). The intermediate frequencies domain, for both relaxation moduli, indicates clearly the appearance of two plateau regimes. In Fig. 6 for the largest generation considered, namely $N = 3^8 \cdot 4^8$, the approximate values of α' at the plateaus are 0.56 and 0.68, in very good agreement with the values of α_V and α_S obtained for $G'(\omega)$ (Fig. 4). Also, in Fig. 7 for the largest generation considered, namely $N = 3^8 \cdot 4^8$, the approximate values of α'' at the plateaus are 0.56 and 0.68, in very in good agreement with the values of α_V and α_S obtained for $G''(\omega)$ (Fig. 5). In both figures oscillations due to the local structure and multihierarchical construction are also evident.

V. CONCLUSIONS

In the present work we have analyzed the scaling behavior of a new multihierarchical structure. We have built the structure by replicating the Vicsek fractal in the shape of the dual Sierpinski gasket. The calculations have been performed in the framework of generalized Gaussian structures, which are the extensions of the simple Rouse model to complex geometries. As we mentioned in Sec. I excluded volume interactions, entanglement effects, and hydrodynamic interactions were neglected. By including the hydrodynamic interactions the first inconvenience is that the eigenvalues of the product matrix **HA** (**H** being the mobility matrix [4,12]) cannot be determined iteratively. This restricts us to the investigation of the relaxation quantities at small generations of the multihierarchical structure because the eigenvalues must be calculated by numerical diagonalizations and for matrices larger than 5000×5000 the numerical diagonalizations are by no means trivial. Furthermore, for fractal structures which present loops [48], as our multihierarchical structure, the inclusion of the hydrodynamic interactions leads to the loss of scaling in the intermediate time and frequency domains for both relaxation moduli and averaged monomer displacement. The advantage of using the GGS model is that it allows one, in principle, to determine the full dynamical behavior of the structure by making use of only the eigenvalues of its connectivity matrix. Following the iterative method for the determination of the eigenvalues of the dual Sierpinski gasket, developed by Ref. [46], and the iterative method for the determination of eigenvalues of the Vicsek fractal, developed by Refs. [20,21] and complemented with the additional transformation to have

a complete decimation of the structure, we have calculated the whole eigenvalue spectrum at any generation of the multihierarchical structure. With the eigenvalues obtained iteratively we have evaluated basic experimental quantities. The quantities considered have been the stretching of the macromolecules under local external forces, $\langle Y(t)\rangle$, as well as the mechanical relaxation moduli, $G'(\omega)$ and $G''(\omega)$. Interestingly, we have found for both relaxation quantities that the intermediate (time or frequency) domain is composed of two scaling regions, one corresponding to the Vicsek fractal and the other corresponding to the dual Sierpinski gasket. As we already showed, the slopes within these regions depend strongly on the spectral dimensions. Furthermore, the scaling relations found for the dual Sierpinski gasket and the Vicsek fractals treated separately are preserved by the multihierarchical structure. The geometry of the multihierarchical structure is well reflected by its dynamical behavior.

ACKNOWLEDGMENTS

Special thanks are addressed to Prof. A. Blumen for many fruitful discussions. A.J. acknowledges the support of CNCSIS-UEFISCSU, Project No. RP-14 NR 2/1.07.2009. A.V. thanks professor Federico Magnani for use of the computer facilities. The discussions with Dr. M. Galiceanu were very helpful.

APPENDIX

As we mentioned in Sec. III, to attain the generation $g \geqslant 1$ and $l = 0$ an additional transformation is needed. This transformation is as follows: every three connected Vicsek fractals of generation $l = 1$ have to be reduced to a dual Sierpinski gasket at generation $g = 1$. The situation is sketched in Fig. 8. We follow here the method developed by Ref. [21]. As in Ref. [21] our starting point is Eq. (10), which gives the relations between the components ϕ of the eigenvector Φ belonging to a certain eigenvalue λ. The eigenvalue equations we needed for our calculations are

$$(3-\lambda)\phi_{10} = \phi_{11} + \phi_{12} + \phi_{13}, \tag{A1}$$

$$(1-\lambda)\phi_{11} = \phi_{10}, \tag{A2}$$

$$(2-\lambda)\phi_{12} = \phi_{10} + \phi_{21}, \tag{A3}$$

$$(2-\lambda)\phi_{13} = \phi_{10} + \phi_{31}, \tag{A4}$$

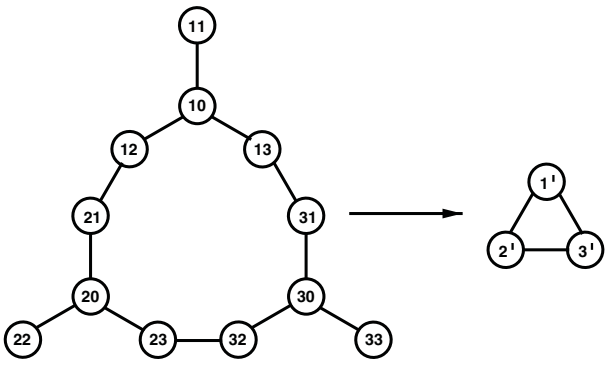

FIG. 8. Decimation step from the generation $g = 1$ and $l = 1$ to the generation $g = 1$ and $l = 0$.

$$(3-\lambda)\phi_{20} = \phi_{21} + \phi_{22} + \phi_{23}, \tag{A5}$$

$$(2-\lambda)\phi_{21} = \phi_{20} + \phi_{12}, \tag{A6}$$

$$(3-\lambda)\phi_{30} = \phi_{31} + \phi_{32} + \phi_{33}, \tag{A7}$$

$$(2-\lambda)\phi_{31} = \phi_{30} + \phi_{13}. \tag{A8}$$

By inserting Eqs. (A2), (A3), and (A4) into Eq. (A1) one obtains

$$(3-\lambda)\phi_{10} = \frac{\phi_{10}}{1-\lambda} + \frac{\phi_{10}+\phi_{21}}{2-\lambda} + \frac{\phi_{10}+\phi_{31}}{2-\lambda} \tag{A9}$$

and with few algebraic calculations one has

$$(-\lambda^3 + 6\lambda^2 - 8\lambda + 2)\phi_{10} = (1-\lambda)\phi_{21} + (1-\lambda)\phi_{31}. \tag{A10}$$

Rewriting the expression $-\lambda^3 + 6\lambda^2 - 8\lambda + 2$ as $-\lambda^3 + 7\lambda^2 - \lambda^2 - 12\lambda + 4\lambda + 2$, while adding and subtracting ϕ_{21} and ϕ_{31}, leads to

$$[2-(\lambda^3 - 7\lambda^2 + 12\lambda)]\phi_{10} = \lambda^2\phi_{10} - 4\lambda\phi_{10} + (2-\lambda)\phi_{21} - \phi_{21} + (2-\lambda)\phi_{31} - \phi_{31}. \tag{A11}$$

Making use of Eqs. (A6) and (A8) on the right-hand side of Eq. (A11) and, also, remarking that $\lambda^3 - 7\lambda^2 + 12\lambda$ is exactly the polynomial $P(\lambda)$ from Eq. (18), we get

$$[2-P(\lambda)]\phi_{10} = \lambda^2\phi_{10} - 4\lambda\phi_{10} + \phi_{12} + \phi_{13} + \phi_{20} - \phi_{21} + \phi_{30} - \phi_{31}. \tag{A12}$$

Combining Eqs. (A1), (A2), and (A3) leads to

$$(-\lambda^3 + 6\lambda^2 - 10\lambda + 4)\phi_{11} = \phi_{10} + \phi_{21} + (2-\lambda)\phi_{13}. \tag{A13}$$

By rewriting expression $-\lambda^3 + 6\lambda^2 - 10\lambda + 4$ as $-\lambda^3 + 7\lambda^2 - \lambda^2 - 12\lambda + 2\lambda + 2 + 2$ and using Eq. (A4), Eq. (A3) yields

$$[2-(\lambda^3 - 7\lambda^2 + 12\lambda)]\phi_{11} = \lambda^2\phi_{11} - 2\lambda\phi_{11} - 2\phi_{11} + 2\phi_{10} + \phi_{21} + \phi_{31}. \tag{A14}$$

Now, identifying $\lambda^3 - 7\lambda^2 + 12\lambda$ with $P(\lambda)$ from Eq. (18), one obtains

$$[2-P(\lambda)]\phi_{11} = \lambda^2\phi_{11} - 2\lambda\phi_{11} - 2\phi_{11} + 2\phi_{10} + \phi_{21} + \phi_{31}. \tag{A15}$$

Inserting Eqs. (A1) and (A6) into Eq. (A3) results in

$$(-\lambda^3 + 7\lambda^2 - 14\lambda + 7)\phi_{12} = (2-\lambda)\phi_{11} + (2-\lambda) \times \phi_{13} + (3-\lambda)\phi_{20}. \tag{A16}$$

Rewriting in Eq. (A16) the expressions $-\lambda^3 + 7\lambda^2 - 14\lambda + 7$ as $-\lambda^3 + 7\lambda^2 - 12\lambda - 2\lambda + 2 + 5$ and $(2-\lambda)\phi_{11}$ as $(1-\lambda)\phi_{11} + \phi_{11}$ one has

$$[2-(\lambda^3 - 7\lambda^2 + 12\lambda)]\phi_{12} = 2\lambda\phi_{12} - 5\phi_{12} + (1-\lambda) \times \phi_{11} + \phi_{11} + (2-\lambda) \times \phi_{13} + (3-\lambda)\phi_{20}. \tag{A17}$$

Using Eqs. (A2), (A4), and (A5) on the right-hand side of Eq. (A17), and again identifying the polynomial $P(\lambda)$ from Eq. (18), one obtains

$$[2 - P(\lambda)]\phi_{12} = 2\phi_{10} + \phi_{11} + 2\lambda\phi_{12} - 5\phi_{12} + \phi_{21} + \phi_{22} + \phi_{23} + \phi_{31}. \quad \text{(A18)}$$

Inserting Eqs. (A1) and (A8) into Eq. (A4) leads to

$$(-\lambda^3 + 7\lambda^2 - 14\lambda + 7)\phi_{13} = (2 - \lambda)\phi_{11} + (2 - \lambda) \times \phi_{12} + (3 - \lambda)\phi_{30}. \quad \text{(A19)}$$

Again, rewriting the expressions $-\lambda^3 + 7\lambda^2 - 14\lambda + 7$ as $-\lambda^3 + 7\lambda^2 - 12\lambda - 2\lambda + 2 + 5$ and $(2 - \lambda)\phi_{11}$ as $(1 - \lambda)\phi_{11} + \phi_{11}$ one obtains

$$[2-(\lambda^3-7\lambda^2+12\lambda)]\phi_{13} = 2\lambda\phi_{13} - 5\phi_{13} + (1 - \lambda)\phi_{11} + \phi_{11} + (2 - \lambda)\phi_{12} + (3 - \lambda)\phi_{30}. \quad \text{(A20)}$$

Using Eqs. (A2), (A3), and (A7) on the right-hand side of Eq. (A20), and again identifying the polynomial $P(\lambda)$ from Eq. (18), leads to

$$[2 - P(\lambda)]\phi_{13} = 2\phi_{10} + \phi_{11} + 2\lambda\phi_{13} - 5\phi_{13} + \phi_{21} + \phi_{31} + \phi_{32} + \phi_{33}. \quad \text{(A21)}$$

Summing Eqs. (A12), (A15), (A18), and (A21) leads to

$$[2 - P(\lambda)](\phi_{10} + \phi_{11} + \phi_{12} + \phi_{13}) = 2\phi_{10} - (2 - \lambda)\phi_{12} - (2 - \lambda)\phi_{13} + \phi_{20} + 2\phi_{21} + \phi_{22} + \phi_{23} + \phi_{30} + 2\phi_{31} + \phi_{32} + \phi_{33}. \quad \text{(A22)}$$

We mention that the expressions $\lambda^2\phi_{10} - 4\lambda\phi_{10}$ and $\lambda^2\phi_{11} - 2\lambda\phi_{11}$ were rewritten as

$$\lambda^2\phi_{10} - 4\lambda\phi_{10} = -\lambda(3 - \lambda)\phi_{10} - \lambda\phi_{10} = -\lambda\phi_{11} - \lambda\phi_{12} - \lambda\phi_{13} - \lambda\phi_{10} \quad \text{(A23)}$$

and

$$\lambda^2\phi_{11} - 2\lambda\phi_{11} = -\lambda(1 - \lambda)\phi_{11} - \lambda\phi_{11} = -\lambda\phi_{10} - \lambda\phi_{11}. \quad \text{(A24)}$$

Using Eqs. (A3) and (A4) on the right-hand side of Eq. (A22) leads to

$$[2 - P(\lambda)](\phi_{10} + \phi_{11} + \phi_{12} + \phi_{13}) = \phi_{20} + \phi_{21} + \phi_{22} + \phi_{23} + \phi_{30} + \phi_{31} + \phi_{32} + \phi_{33}. \quad \text{(A25)}$$

From Eq. (A25) it is simple to identify

$$\phi_1' = \phi_{10} + +\phi_{11} + \phi_{12} + \phi_{13}, \quad \text{(A26)}$$

$$\phi_2' = \phi_{20} + +\phi_{21} + \phi_{22} + \phi_{23}, \quad \text{(A27)}$$

$$\phi_3' = \phi_{30} + +\phi_{31} + \phi_{32} + \phi_{33}. \quad \text{(A28)}$$

With results (A26)–(A28), Eq. (A25) reads

$$[2 - P(\lambda)]\phi_1' = \phi_2' + \phi_3', \quad \text{(A29)}$$

which is nothing else than Eq. (19) from Sec. III. In this way, every three connected Vicsek fractals at generation $l = 1$ have been reduced to a dual Sierpinski gasket at generation $g = 1$.

[1] P. E. Rouse, J. Chem. Phys. **21**, 1272 (1953).
[2] B. H. Zimm, J. Chem. Phys. **24**, 269 (1956).
[3] B. Ewen and D. Richter, Adv. Polym. Sci. **134**, 1 (1997).
[4] M. Doi and S. F. Edwards, *The Theory of Polymer Dynamics* (Clarendon, Oxford, 1986).
[5] A. Yu. Grosberg and A. R. Khokhlov, *Statistical Physics of Macromolecules* (American Institue of Physics, New York, 1994).
[6] J. Roovers and B. Comanita, Adv. Polym. Sci. **142**, 179 (1999).
[7] J. Roovers, in *Star and Hyperbranched Polymers*, edited by M. K. Mishra and S. Kobayashi (Dekker, New York, 1999), p. 285.
[8] P. Biswas, R. Kant, and A. Blumen, Macromol. Theory Simul. **9**, 56 (2000).
[9] R. Kant, P. Biswas, and A. Blumen, Macromol. Theory Simul. **9**, 608 (2000).
[10] P. Biswas, R. Kant, and A. Blumen, J. Chem. Phys. **114**, 2430 (2001).
[11] J. Kemp and Z. Y. Chen, Phys. Rev. E **56**, 7017 (1997).
[12] C. Cai and Z. Y. Chen, Macromol. **30**, 5104 (1997).
[13] Z. Y. Chen and C. Cai, Macromol. **32**, 5423 (1999).
[14] W. Burchard, Adv. Polym. Sci. **143**, 113 (1999).
[15] J. J. Freire, Adv. Polym. Sci. **143**, 35 (1999).
[16] F. Ganazzoli, R. La Ferla, and G. Raffaini, Macromol. **34**, 4222 (2001).
[17] C. von Ferber and A. Blumen, J. Chem. Phys. **116**, 8616 (2002).
[18] C. S. Jayanthi, S. Y. Wu, and J. Cocks, Phys. Rev. Lett. **69**, 1955 (1992).
[19] C. S. Jayanthi and S. Y. Wu, Phys. Rev. B **50**, 897 (1994).
[20] A. Blumen, A. Jurjiu, Th. Koslowski, and Ch. von Ferber, Phys. Rev. E **67**, 061103 (2003).
[21] A. Blumen, Ch. von Ferber, A. Jurjiu, and Th. Koslowski, Macromolecules **37**, 638 (2004).
[22] A. Volta, M. Galiceanu, and A. Jurjiu, J. Phys. A **43**, 105205 (2010).
[23] A. A. Gurtovenko and A. Blumen, J. Chem. Phys. **115**, 4924 (2001).
[24] S. Jespersen, I. M. Sokolov, and A. Blumen, J. Chem. Phys. **113**, 7652 (2000).
[25] A. Blumen, A. A. Gurtovenko, and S. Jespersen, J. Non-Cryst. Solids **305**, 71 (2002).
[26] A. A. Gurtovenko and A. Blumen, Adv. Polym. Sci. **182**, 171 (2005).
[27] M. Galiceanu and A. Blumen, J. Phys. Condens. Matter **19**, 065122 (2007).
[28] B. Mandelbrot, *The Fractal Geometry of Nature* (Freeman, San Francisco, 1982).
[29] J.-U. Sommer and A. Blumen, J. Phys. A **28**, 6669 (1995).
[30] H. Schiessel, Phys. Rev. E **57**, R5775 (1998).

[31] *Fractals and Disordered Systems*, edited by A. Bunde and S. Havlin (Springer-Verlag, Berlin, 1996).
[32] A. Blumen and A. Jurjiu, J. Chem. Phys. **116**, 2636 (2002).
[33] A. Jurjiu, C. Friedrich, and A. Blumen, Chem. Phys. **284**, 221 (2002).
[34] A. Jurjiu, T. Koslowski, C. von Ferber, and A. Blumen, Chem. Phys. **294**, 187 (2003).
[35] A. Blumen, A. Volta, A. Jurjiu, and T. Koslowski, Physica A **356**, 12 (2005).
[36] G. Allegra and F. Ganazzoli, Adv. Chem. Phys. **75**, 265 (1989).
[37] H. Schiessel, C. Friedrich, and A. Blumen, in *Applications of Fractional Calculus in Physics* edited by R. Hilfer (World Scientific, Singapore, 2000), p. 331.
[38] I. M. Ward, *Mechanical Properties of Solid Polymers*, 2nd ed. (Wiley, Chichester, 1985).
[39] J. D. Ferry, *Viscoelastic Properties of Polymers*, 3rd ed. (Wiley, New York, 1980).
[40] T. T. Perkins, D. E. Smith, R. G. Larson, and S. Chu, Science **268**, 83 (1995).
[41] D. Wirtz, Phys. Rev. Lett. **75**, 2436 (1995).
[42] S. R. Quake, H. Babcock, and S. Chu, Nature (London) **388**, 151 (1997).
[43] F. Amblard, A. C. Maggs, B. Yurke, A. N. Pergellis, and S. Leibler, Phys. Rev. Lett. **77**, 4470 (1996).
[44] J. W. Hatfield and S. R. Quake, Phys. Rev. Lett. **82**, 3548 (1999).
[45] E. Helfer, S. Harlepp, L. Bourdieu, J. Robert, F. C. MacKintosh, and D. Chatenay, Phys. Rev. Lett. **85**, 457 (2000).
[46] M. G. Cosenza and R. Kapral, Phys. Rev. A **46**, 1850 (1992).
[47] I. N. Bronstein and K. A. Semendjajev, *Taschenbuch der Mathematik* (Nauka and Teubner, Moscow and Leipzig, 1985), Chap. 2.4.2.
[48] A. Jurjiu, Th. Koslowski, and A. Blumen, J. Chem. Phys. **118**, 2398 (2003).